ISSN No:-2456-2165 https://doi.org/10.38124/ijisrt/26may1642

Synthesis of Coal Fly Ash Derived Bromosodalite (Br-SOD) for Efficient Adsorptive Removal of Pb(II), Hg(II), and Cu(II) Ions from Aqueous Solutions

Surekha B. Ghorpade[1]; Rajendra P. Patil[2]; Ashok V. Borhade[3]

[1]Research Centre, Department of Chemistry, K.T.H.M. College (Affiliated to S. P. Pune University), Gangapur Road, Nashik-422002, Maharashtra, India
[1,2]C.H.M.E. Society's, Bhonsala Military College, Nashik-422005, Maharashtra, India
[3]Research Centre, Department of Chemistry, H.P.T. Arts and R.Y. K. Science College, Nashik-422005, Maharashtra, India

Publication Date: 2026/06/02

Abstract: The increasing release of toxic heavy metals into aquatic environments due to rapid industrialization raises serious environmental and public health issues worldwide. In this study, mesoporous bromosodalite (BR-SOD) was successfully produced from coal fly ash using a cost-effective and sustainable hydrothermal method. It was tested as an adsorbent for removing hazardous Pb^{2+}, Hg^{2+}, and Cu^{2+} ions from water. The material was thoroughly characterized with techniques such as Fourier Transform Infrared Spectroscopy (FTIR), X-ray Diffraction (XRD), Brunauer–Emmett–Teller (BET) surface area analysis, Field Emission Scanning Electron Microscopy (FE-SEM), High-Resolution Transmission Electron Microscopy (HR-TEM), and Energy Dispersive X-ray Spectroscopy (EDS) mapping to examine its structural, morphological, and surface features. Characterization confirmed the successful formation of crystalline bromosodalite with a highly mesoporous structure, greatly improving its ability to adsorb metal ions. Batch experiments were performed to optimize key operational parameters such as pH, adsorbent dose, initial metal ion concentration, contact time, and temperature. These experiments were conducted at three temperatures: 301.15 K, 323.15 K, and 343.15 K. The equilibrium data were modelled using the Langmuir isotherm, and the resulting parameters clarified the adsorption mechanism. The synthesized BR-SOD showed excellent ability to adsorb and a high affinity for Pb^{2+}, Hg^{2+}, and Cu^{2+} ions, thanks to its large surface area, porous structure, and plentiful active sites. Results indicate that bromosodalite derived from coal fly ash is a cost-effective, efficient, and environmentally friendly adsorbent for removing toxic heavy metals from wastewater. This research presents a valuable method for transforming industrial waste into useful materials for environmental cleanup.

Keywords: *Sodalite; Adsorption; Isotherms; Mesoporous; Langmuir.*

How to Cite: Surekha B. Ghorpade; Rajendra P. Patil; Ashok V. Borhade (2026) Synthesis of Coal Fly Ash Derived Bromosodalite (Br-SOD) for Efficient Adsorptive Removal of Pb(II), Hg(II), and Cu(II) Ions from Aqueous Solutions.
International Journal of Innovative Science and Research Technology, 11(5), 2796-2805.
https://doi.org/10.38124/ijisrt/26may1642

I. INTRODUCTION

Rapid industrialization and urban growth have markedly increased the release of hazardous heavy metals into water sources, causing serious environmental pollution and health issues [1-8]. Metals like lead [Pb^{2+}], mercury [Hg^{2+}], and copper [Cu^{2+}] are highly toxic because they are non-biodegradable, persistent, and tend to bioaccumulate. These toxic metal ions are released into the environment through various industrial processes, including mining, electroplating, battery manufacturing, [9-15] metal finishing, paint and pigment production, petroleum refining, fertilizer production, chlor-alkali processing, textile treatment, electronic waste recycling, and chemical manufacturing. Lead contamination mainly arises from battery manufacturing, pigments, plumbing, and mining activities [16-21]. Exposure to Pb^{2+} can result in serious neurological problems, kidney issues, anemia, developmental delays in children, and reproductive system damage [22-24]. Mercury contamination is often linked to chlor-alkali plants, pharmaceuticals, mining, and fossil fuel burning [25-28]. Hg^{2+} is highly toxic even at low levels, potentially causing brain damage, nervous system disorders, kidney failure, and ecological disruption through biomagnification in aquatic food chains [29-31]. Copper, while an essential trace element, becomes very toxic at high concentrations and is widely released from electroplating, alloy production, wire manufacturing, and cleaning industries [32-34]. Excess Cu^{2+} exposure can cause liver damage, gastrointestinal issues, and environmental harm to aquatic life. Because of the harmful effects of these heavy metals on

ISSN No:-2456-2165 https://doi.org/10.38124/ijisrt/26may1642

humans and ecosystems, it is crucial to implement effective wastewater treatment technologies before industrial effluents reach natural water bodies [35-36]. Traditional methods like chemical precipitation, ion exchange, membrane filtration, coagulation-flocculation, reverse osmosis, and electrochemical treatment have been used to eliminate heavy metals [37-38]. Nonetheless, these approaches often face challenges such as high operational costs, sludge production, suboptimal removal efficiency, and complex procedures. Among the available technologies, adsorption has emerged as one of the most effective, economical, and environmentally friendly techniques for heavy metal remediation, owing to its simplicity, high efficiency, regenerability, and ease of operation [39-40]. Recently, zeolitic materials and sodalite-based adsorbents have attracted considerable attention for their high surface area, porous framework, ion exchange capacity, and excellent adsorption properties [41-43]. Coal fly ash, a major byproduct of thermal power plants, is generated in enormous quantities worldwide and poses serious disposal and environmental challenges. Since coal fly ash contains substantial amounts of silica and alumina, it serves as an excellent precursor for synthesising zeolitic materials. Converting fly ash into value-added adsorbents not only minimises industrial waste disposal problems but also contributes towards sustainable environmental management [43-44]. Multiple studies have documented the synthesis of zeolites and sodalite materials derived from fly ash for pollutant removal. Literature shows that porous sodalite exhibits excellent adsorption capabilities for toxic metal ions, thanks to its crystalline aluminosilicate structure and ion exchange properties [45-46]. Nevertheless, the creation of mesoporous bromosodalite with improved adsorption efficiency for the concurrent removal of Pb^{2+}, Hg^{2+} and Cu^{2+} ions is still limited. In this study, bromosodalite (BR-SOD) was successfully synthesised from coal fly ash and characterised using FTIR, XRD, BET surface area analysis, FE-SEM, HR-TEM, and EDS elemental mapping. The mesoporous BR-SOD was evaluated as an efficient adsorbent for removing Pb^{2+}, Hg^{2+}, and Cu^{2+} ions from aqueous solution through batch adsorption studies. Key operational parameters, including pH, adsorbent dose, contact time, initial metal ion concentration, and temperature, were optimised. Furthermore, adsorption equilibrium behaviour was evaluated using the Langmuir adsorption isotherm model at temperatures of 301.15 K, 323.15 K, and 343.15 K. The study demonstrates that coal fly ash-derived bromosodalite is a promising, low-cost, and sustainable adsorbent for heavy metal wastewater treatment applications.

II. MATERIALS AND METHODS

➢ *Material*

The primary precursor for synthesis, Coal Fly Ash (CFA), was sourced from the Nashik Thermal Power Station in Eklahara, Nashik, Maharashtra, India. This CFA was generated by combusting pulverised bituminous coal and provided a vital source of reactive silica (SiO_2) and alumina (Al_2O_3). Potassium bromide (KBr) of 99.9% purity was purchased from Sigma-Aldrich and serves as a structure-directing agent. Sodium Hydroxide (NaOH) of 99% purity was acquired from Sigma-Aldrich and served as an activating agent. Heavy metal ion salts- CuSO4, HgCl2, and Pb(NO3)2- each 99% pure, were obtained from Sigma-Aldrich. Double-distilled water was used throughout all synthesis and experimental procedures. All chemicals were used as received, without further purification.

➢ *Synthesis of Br-SOD*

The collected CFA was carefully purified by rinsing with dilute Nitric Acid (HNO_3) and double-distilled water to remove acid-soluble metal oxides and trace elements, including Fe, Ca, Mg, and unburned carbon. During this process, magnetic parts were separated and removed using a high-intensity magnetic stirrer and external magnets. The purified CFA was then filtered and dried to a constant weight in a laboratory oven. Synthesis began with a subcritical fusion method, in which cleaned CFA was mixed with Sodium Hydroxide (NaOH) at a 1:1 weight ratio and heated in a silica crucible at 550 °C for 2 hours in a muffle furnace. The fused material was dispersed in distilled water (1 g in 10 mL) with vigorous stirring. To this slurry, 7 g of KBr was added as a structure-directing agent. The mixture was transferred into a stainless-steel-lined Teflon autoclave and treated hydrothermally at 120°C for 6 days. The resulting creamy white polycrystalline bromosodalite, $Na_8[AlSiO_4]_6Br_2$, was collected by filtration, washed with deionised water until reaching a neutral pH, and then dried at 100°C for 24 hours, as shown in Figure 1. The bromosodalite framework was finalised after calcination at 550°C and named as Br-SOD[47].

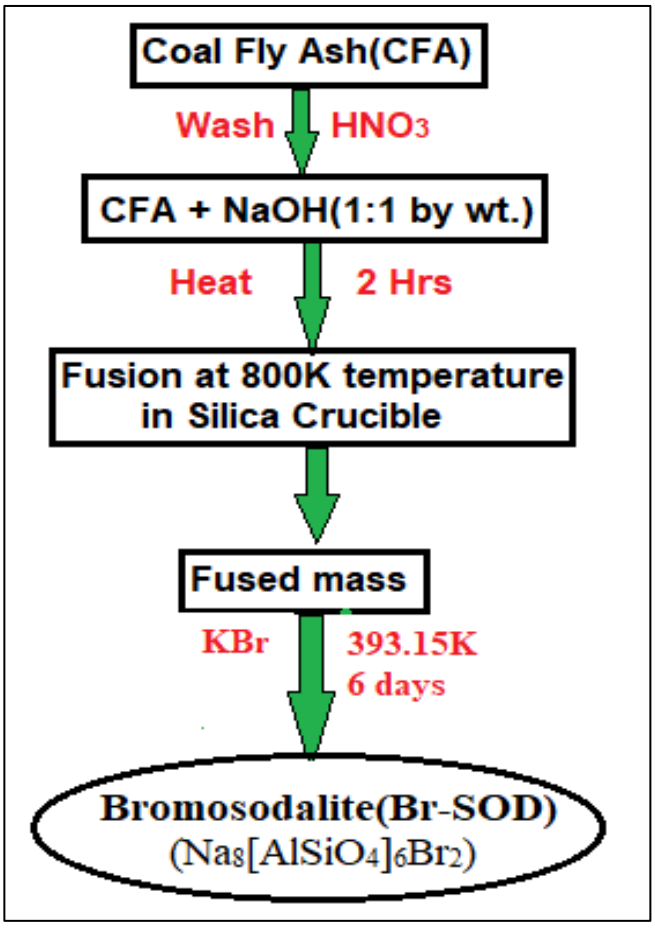

Fig 1 Flow Chart of Synthesis of Bromosodalite

ISSN No:-2456-2165 https://doi.org/10.38124/ijisrt/26may1642

➢ *Characterization Techniques*

A comprehensive multi-analytical approach was employed to characterise the structural, optical, and morphological features of the synthesised catalysts. X-ray Diffraction (XRD) determined the crystalline phases and lattice constants. Fourier Transform Infrared (FT-IR) spectroscopy identified characteristic framework vibrations and functional groups associated with the sodalite structure. Field Emission Scanning Electron Microscopy (FE-SEM) was used to analyse surface morphology, particle size distribution, and aggregation states. This analysis was supported by Energy Dispersive X-ray (EDX) spectroscopy and elemental mapping, which verified the chemical composition and the uniform distribution of metal oxides. High-Resolution Transmission Electron Microscopy (HR-TEM) provided detailed structural insights, visualising lattice fringes and confirming atomic-level crystallinity.

➢ *Metal Ion Removal Experimental Set-up*

To verify the Langmuir adsorption isotherm and explore its parameters- including solution pH, initial metal ion concentration, amount of adsorbent (Br-SOD), and contact time- individual metal ions were studied using the batch adsorption method. The metal ion adsorption capacity of Br-SOD was assessed with equation 1, and the adsorbent's capacity was calculated using equation 2.

$$\%\ Adsorption = \frac{C0 - Ce}{C0}\ x\ 100 - - - - - - - - - Eq.1$$

$$Qe = \frac{C0 - Ce}{m}\ x\ V - - - - - - - - - - - - - - - - Eq.2$$

- *Effect of pH Variation*

An essential parameter in studying the adsorption of metal ions such as Cu^{2+}, Hg^{2+}, and Pb^{2+} onto Br-SOD is the solution pH. To analyse the effects of pH, 25 mL of a metal-ion solution at a specific concentration was placed in multiple stoppered glass bottles. Each bottle received a standard buffer solution at pH 1, 3, 5, 7, 9, and 11, along with 0.250 g of Br-SOD adsorbent. The bottles were then incubated in an oven at a fixed temperature for 2 hours, with intermittent shaking to reach equilibrium. Afterwards, the contents were filtered, and the filtrates were titrated with $1x10^{-3}$M EDTA solution in the presence of a pH 10 buffer solution using Eriochrome Black T (EBT) as the indicator.

- *Effect of Contact Time Variation*

The study measured the percentage of metal ions removed over time using 25 mL of 0.001 M metal-ion solutions in glass-stoppered bottles. To each bottle, 5 mL of buffer solution was added, with pH 7 for Pb^{2+} and pH 8 for Cu^{2+} and Hg^{2+}. Then, 0.250 g of Br-SOD adsorbent was introduced, and the bottles were placed in an oven at the desired temperature. The solutions were stirred thoroughly until equilibrium was achieved, then filtered at various contact times (0, 30, 60, 90, 120, 150, 180, and 240 minutes) using Whatman filter paper. The filtrates were then titrated with 0.001 M EDTA, in the presence of a pH 10 buffer solution, using Eriochrome Black T (EBT) as the indicator.

- *Effect of Initial Metal Ion Concentration Variation*

Solutions of varying concentrations were prepared by diluting the stock metal salt solution with distilled water. Exactly 25 mL of each solution was transferred to 100 mL stoppered bottles. 5 ml of buffer at the desired pH was added to each bottle. Next, 0.250 g of Br-SOD adsorbent was introduced, and the bottles were placed in an oven at the specified temperature for 3 hours. The bottles were shaken at regular intervals to ensure equilibrium. After equilibrium, the solutions were filtered through Whatman filter paper. The filtrates were titrated with 0.001 M EDTA solution in the presence of a pH 10 buffer solution using Eriochrome Black T (EBT) as the indicator.

- *Effect of Adsorbent dose Variation*

To investigate the effect of adsorbent dose of Br-SOD, 50 mL of metal ion solution having an initial concentration of 100 mg/L was taken in a series of glass-stoppered bottles. To each bottle, 5 mL of buffer solution of the desired pH was added. Different amounts of Br-SOD adsorbent, ranging from 0.1 to 1.0 g, were added to the respective bottles. The bottles were then kept in an oven at the desired constant temperature for 3 hours. During this period, the solutions were intermittently shaken to reach equilibrium. After equilibration, the solutions were filtered using Whatman filter paper. The filtrates were titrated against $1x10^{-3}$ M EDTA solution in presence of pH 10 buffer solution using Eriochrome Black T (EBT) as the indicator.

III. RESULTS AND DISCUSSION

➢ *FTIR*

FTIR of raw coal fly ash and synthesized bromosodalite were reported as shown in figure 2. a) Br-SOD and b) CFA significate changes are given in table.1

Table 1 FTIR Data for Bromosodalite and CFA

Wavenumber (cm^{-1})	Assignment/Functional Group	Structural Evolution
2350 (a)	Asymmetric (CO2) stretch	Appears; indicates ambient (CO2) adsorption/trapping in sodalite cages
1400 / 1320 (b)	Amorphous silicate/carbonate impurities	Disappears, which signifies complete dissolution of the raw fly ash phase
1000 (a and b)	Asymmetric (T-O-T) (T = Si, Al) stretching	Sharpens intensely, it confirms highly crystalline sodalite framework formed
720 (a)	Symmetric (T-O-T) stretching	Appears cleanly and identifies the definitive sodalite secondary building units

ISSN No:-2456-2165 https://doi.org/10.38124/ijisrt/26may1642

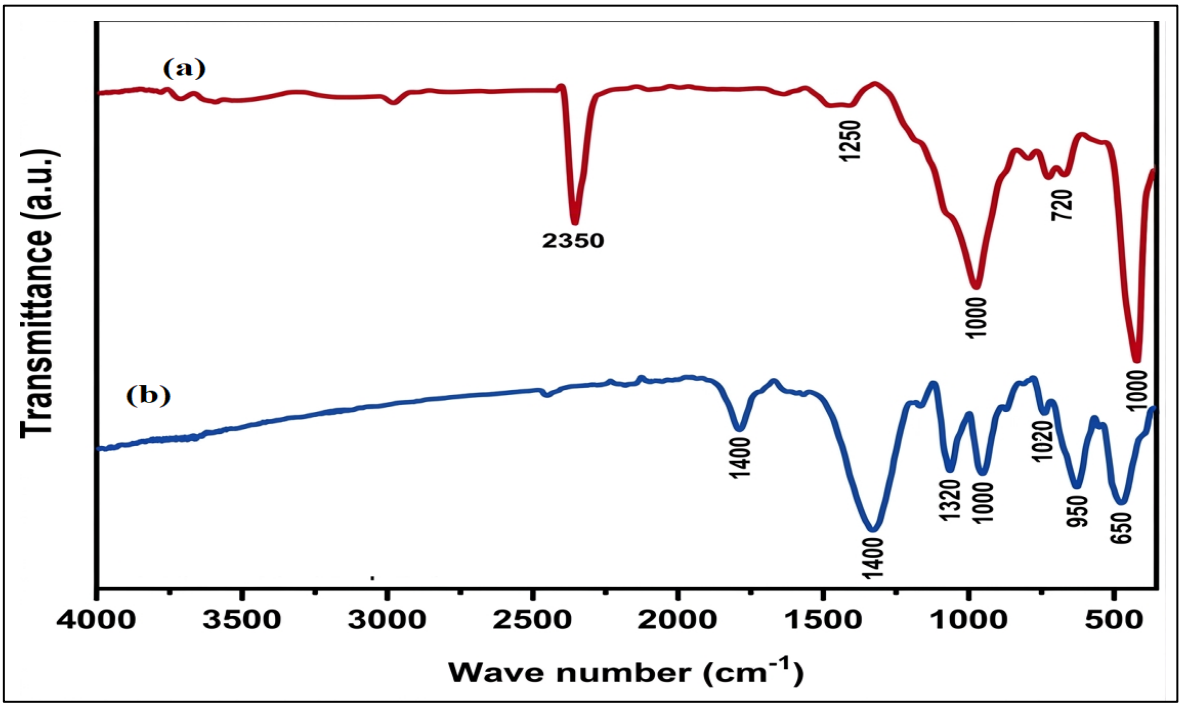

Fig 2 FTIR Spectral Analysis for a) Bromosodalite b) Coal Fly Ash

The successful transformation is evidenced by a complete reorganization of the aluminosilicate framework from a disordered state to a well-defined crystalline structure. In the raw coal fly ash spectrum (Figure 2b), the material shows broad, poorly resolved bands, particularly the wide features around 1400 cm^{-1}, 1320 cm^{-1}, and 1020–950 cm^{-1}—which are typical of amorphous silicate glass, quartz, and mullite components present in raw ash. After alkaline hydrothermal treatment with bromide ions, this amorphous pattern vanishes, revealing the sharp vibrational signature of bromosodalite (Figure 2a). The key evidence of crystallisation is the appearance of a strong, narrow asymmetric (T-O-T) (T = Si, Al) tetrahedral stretching band centred at 1000 cm^{-1}, along with distinct symmetric framework vibrations at 720 cm^{-1}. Additionally, a prominent and sharp peak at 2350 cm ^{1}, unique to the Br-SOD spectrum, indicates the asymmetric stretching vibration of CO_2 molecules adsorbed onto the crystalline framework or trapped in sodalite cages during synthesis and handling. This notable change from a broad, multi-peaked amorphous pattern to sharp, isolated crystalline bands confirms that the raw coal fly ash has been fully converted into well-structured aluminosilicate framwork, Br-SOD.

➢ *X-ray Diffraction (XRD)*

The crystalline evolution is demonstrated by the complete phase restructuring shown between the raw material and the synthesized product in Figure 3 a) Br-SOD and b) CFA. In table 2 principle peaks are illustrated in detailed.

Table 2 Characteristic XRD Peaks for Synthesized Br-SOD and CFA

Peak Position (2θ)	Mineral Phase / Crystalline Assignment	Structural Evolution
15° - 30° (Hump)	Amorphous aluminosilicate glass matrix	Flattens completely; signifies total dissolution of the disordered ash phase
14.1°	Bromosodalite symmetric reflection	Appears sharply; marks initial long-range crystalline ordering
24.3°	Primary Bromosodalite skeletal reflection	Emerges as the highest intensity peak; confirms successful cage framework growth
26.6°	Residual Quartz (SiO2) impurity	Disappears/diminishes; shows consumption of raw minerals into synthesis precursors
34.8° / 43.2°	Secondary Bromosodalite cubic reflections	Emerge clearly; confirm high phase purity and high crystallinity of the sodalite

ISSN No:-2456-2165 https://doi.org/10.38124/ijisrt/26may1642

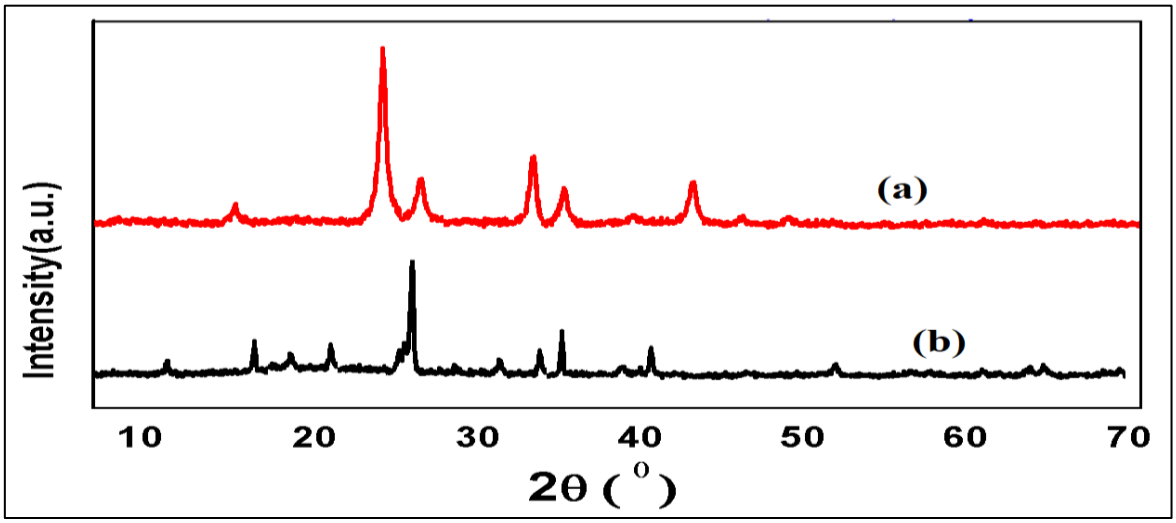

Fig 3 XRD Pattern of a) Bromosodalite b) Coal Fly Ash

The raw coal fly ash XRD pattern Figure 3b is characterised by a broad, elevated background amorphous hump centred between 15° and 30° 2θ), which represents the disordered vitrified aluminosilicate glass phase dominant in industrial fly ash. Superimposed on this amorphous background are sharp, narrow diffraction reflections—most notably the highly intense peak positioned near 26.6°(2θ)—which signify the presence of unreacted inert crystalline impurities like quartz (SiO_2) and mullite ($Al_6Si_2O_{13}$). Upon undergoing alkaline hydrothermal activation and conversion, the synthesized bromosodalite pattern Figure 3a exhibits a flat baseline entirely free of the amorphous halo, proving that the disordered glass phase has completely dissolved. It is replaced by an array of intense, sharp, and well-resolved Bragg reflections characteristic of a highly ordered cubic sodalite framework. The defining peaks of the newly formed bromosodalite phase emerge prominently at 14.1°, a dominant peak at 24.3°, followed by stable structural peaks at 31.8°, 34.8°, and 43.2° (2θ). The complete disappearance of the primary quartz peak at 26.6°C indicates that the initial ash matrix was effectively consumed as a source of silicon and aluminium to build the crystalline cages of the aluminosilicate, Br-SOD framework.

➢ *Morphological Characterization*

The morphological evolution captured by Scanning Electron Microscopy (SEM) demonstrates a distinct structural transition from raw material to synthesized product, shown in figure 4. a) SEM image of CFA b) SEM image of Br-SOD.

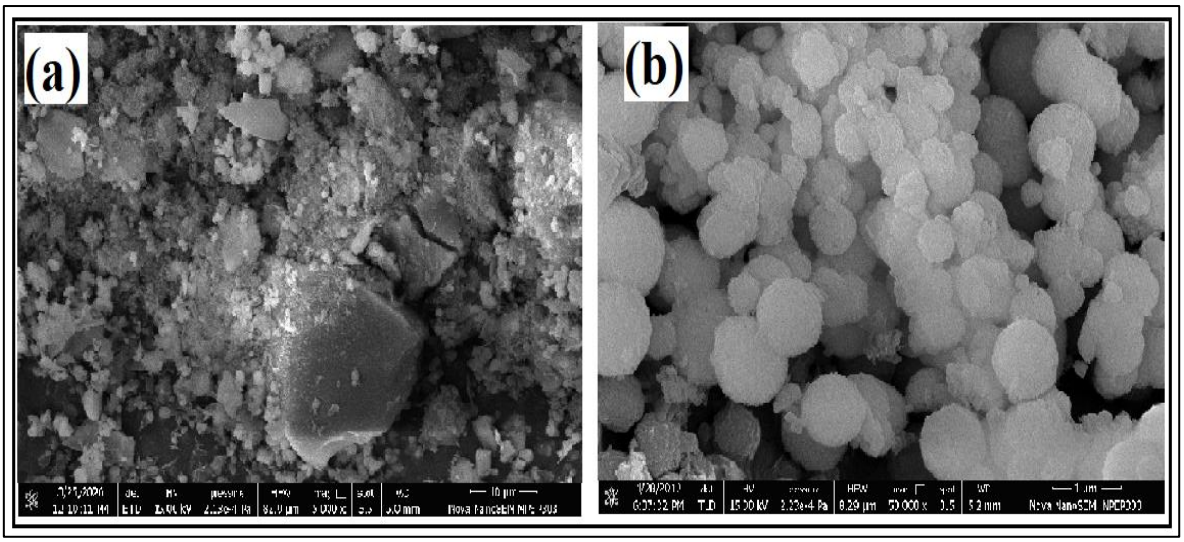

Fig 4 FE-SEM Pattern of a) Coal Fly Ash b) Bromosodalite

The FE-SEM micrograph of raw coal fly ash shown in Figure 4a reveals the heterogeneous morphological nature of the precursor material, which is primarily composed of irregularly distributed particles with ranges of sizes and shapes. CFA The surface morphology of coal fly ash generally consists of smooth spherical particles, cenospheres, porous fragments, and agglomerated aluminosilicate phases generated during high-temperature coal combustion in thermal power plants. Many particles exhibit glassy and relatively non-porous surfaces, indicating the presence of amorphous aluminosilicate materials along with some crystalline impurities such as quartz and mullite. The

ISSN No:-2456-2165 https://doi.org/10.38124/ijisrt/26may1642

spherical morphology observed in fly ash particles originates from the melting and rapid solidification of mineral matter during formation. In addition, some unburned carbon particles and rough-textured fragments can also be observed, contributing to the heterogeneous structure of the raw material. The dense and compact morphology of coal fly ash indicates limited active adsorption sites and comparatively lower surface area before hydrothermal treatment. However, the presence of reactive silica and alumina phases in the fly ash makes it an excellent precursor for the synthesis of zeolitic materials such as bromosodalite.

The FE-SEM image of the synthesized Br-SOD in Figure 4b reveals a significant change in morphology after hydrothermal synthesis. The Br-SOD displays well-formed crystalline structures with a highly ordered cubic shape, indicating successful formation of bromosodalite from coal fly ash. The micrograph shows numerous fine cubic crystals evenly distributed and connected, forming spherical clusters. These spherical agglomerates result from the self-assembly and aggregation of individual bromosodalite nanocrystals during crystallization under alkaline hydrothermal conditions. The densely packed cubic crystals have intercrystalline voids and channels, creating a mesoporous framework. The clustering into spherical structures boosts surface roughness and porosity. Compared to raw fly ash, the Br-SOD is more porous, loose, and textured, with a larger surface area and interconnected pores. This transformation stems from the dissolution of amorphous aluminosilicate species in fly ash, followed by nucleation and recrystallization into a crystalline sodalite structure. The spherical aggregates of nano- to micro-sized cubic crystals provide extensive external surface area and more accessible adsorption sites, essential for heavy metal ion capture. Additionally, the mesoporous design promotes fast diffusion of Pb^{2+}, Hg^{2+}, and Cu^{2+} ions into internal adsorption sites. The morphological features align with BET surface area results and confirm that the bromosodalite has an optimal surface structure for adsorption. Overall, FE-SEM analysis shows that hydrothermal treatment effectively converts dense, less active fly ash particles into highly crystalline, mesoporous spherical aggregates of cubic bromosodalite crystals, which achieve excellent adsorption of hazardous heavy metals from aqueous solutions.

➢ *Batch Adsorption Study*

To verify the applicability of various adsorption isotherms and to investigate thermodynamic parameters, batch adsorption studies of individual metal ions were carried out. Different experimental parameters such as pH, contact time, initial metal ion concentration, and adsorbent dose were examined at different temperatures.

- *Variation of pH*

In order to study the effect of pH on the extent of adsorption, 25 mL of 1×10^{-3}M metal chloride solutions were taken in a number of stoppered bottles. To these bottles, 5 mL buffer solutions of different pH values (pH = 1, 3, 5, 7, 9.10, 11, and 12) were added. Subsequently, 0.250 g of Br-SOD was added to each bottle. The bottles were kept in an oven at the desired temperature and manually shaken at regular intervals. After 3 hours, the solutions were filtered through Whatman No. 40 filter paper. The filtrates obtained were titrated with 1×10^{-3}M EDTA solution. The percentage adsorption was calculated using Eq. 1 and then plotted as a function of pH in Figure 5.

The careful observation of Figure 5 shows that adsorption increases with increase in pH from 1 to 7 for Pb^{2+} and up to pH 8 for rest of two ions, after which it decreases. This indicates that the optimum pH for the adsorption of Cu^{2+} and Hg^{2+} ions is 8. And for Pb^{2+} ion is 7, Beyond these pH values, the percentage adsorption could not responds due to the formation of precipitates. For further adsorption study, these optimized pH values for respected metal ions are kept constant.

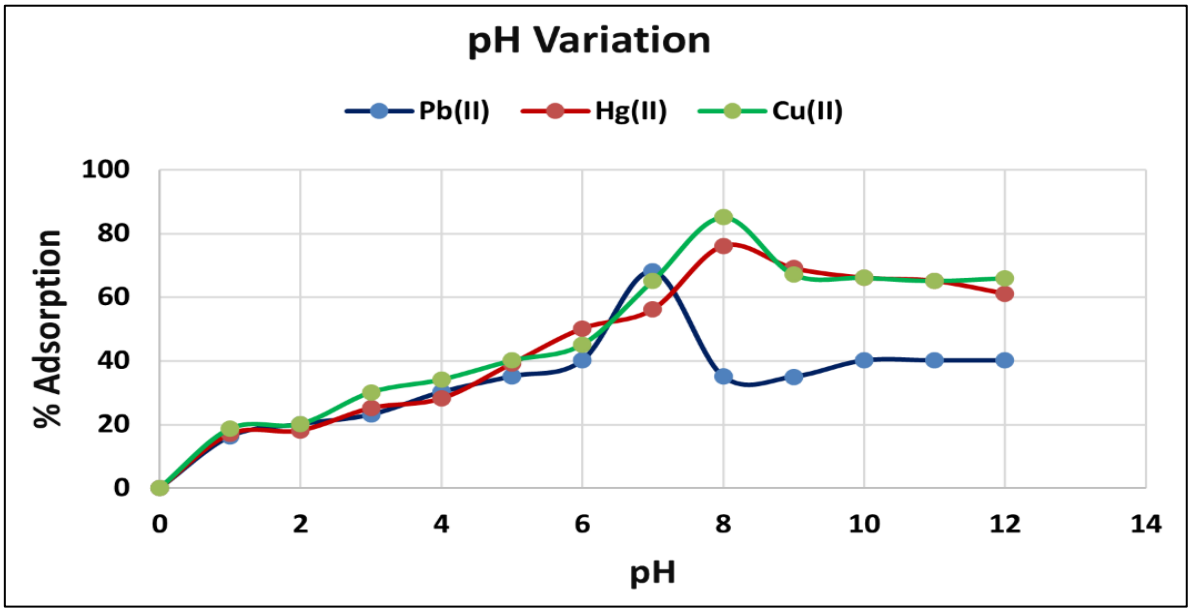

Fig 5 Isotherm of Adsorption of Metal Ions with Varying pH

ISSN No:-2456-2165 https://doi.org/10.38124/ijisrt/26may1642

- *Variation of Contact Time*

The percentage adsorption of Cu^{2+}, Hg^{2+}, and Pb^{2+} ions on Br-SOD was investigated as a function of contact time. The obtained results were plotted against time at different temperatures, namely 303.15, 323.15, and 348.15 K (Figure 6). The optimum uptake of metal ions was achieved within 120 min. A slight decrease in percentage removal after 120 min indicates that the adsorption process had attained equilibrium. Initially, the concentration gradient between the vacant adsorption sites of Br-SOD and the solution phase was very high; therefore, the adsorption rate was rapid during the first few minutes, resulting in nearly 15–40% adsorption. As the vacant sites were occupied by metal ions, the concentration gradient gradually decreased, thereby reducing the adsorption rate. After approximately 120 min, the adsorption rate became constant, confirming the attainment of equilibrium. An increase in temperature enhanced the kinetic energy of the metal ions, thereby facilitating greater diffusion of ions into the pores of Br-SOD and improving adsorption efficiency.

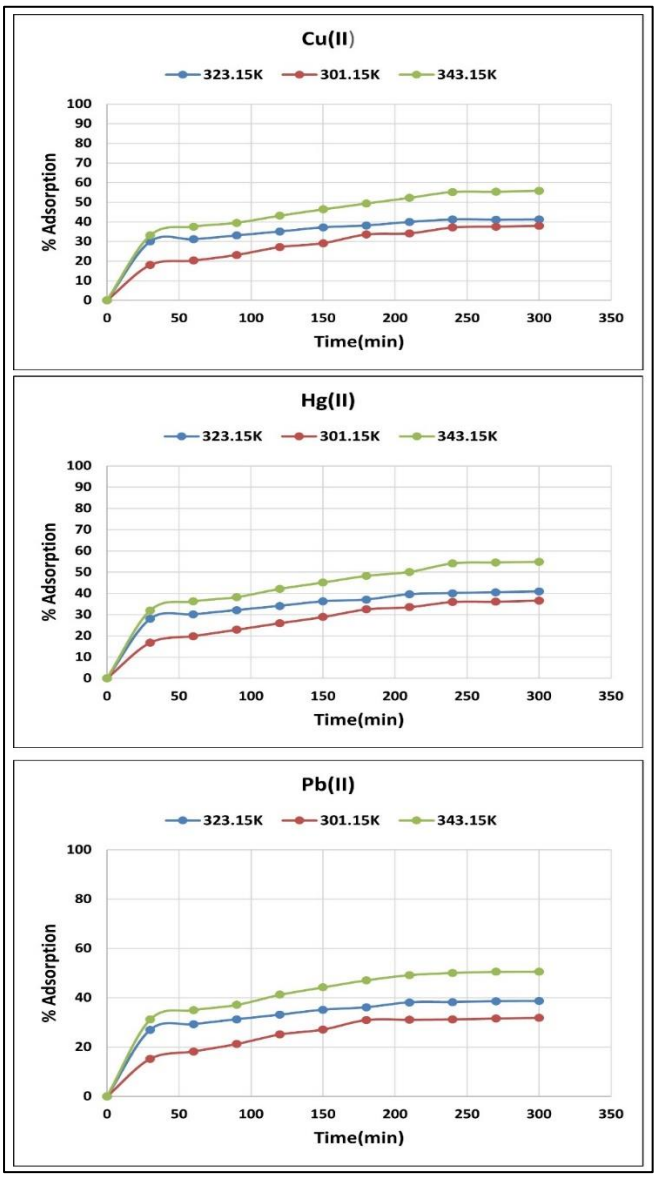

Fig 6 Isotherm of Adsorption of Metal Ions with Varying Contact Time

- *Variation of Metal Ion Concentration*

The effect of the initial metal ion concentration on percentage adsorption was studied at different temperatures (303.15, 323.15, and 348.15 K), and the results are presented in Fig. 7. It was observed that the percentage adsorption initially increased with increasing initial metal ion concentration, reached a maximum, and thereafter remained constant once equilibrium was established. This behaviour can be explained by the availability of vacant adsorption sites and the number of metal ions in the solution phase. For a fixed quantity of adsorbent, the number of adsorption sites remains constant. At lower initial metal-ion concentrations, the number of vacant sites exceeds the number of metal ions in solution, leading to efficient adsorption. As the initial concentration of metal ions increases, more ions compete for the available adsorption sites until saturation is reached. Beyond this point, no significant increase in adsorption is observed because the available adsorption sites become fully occupied.

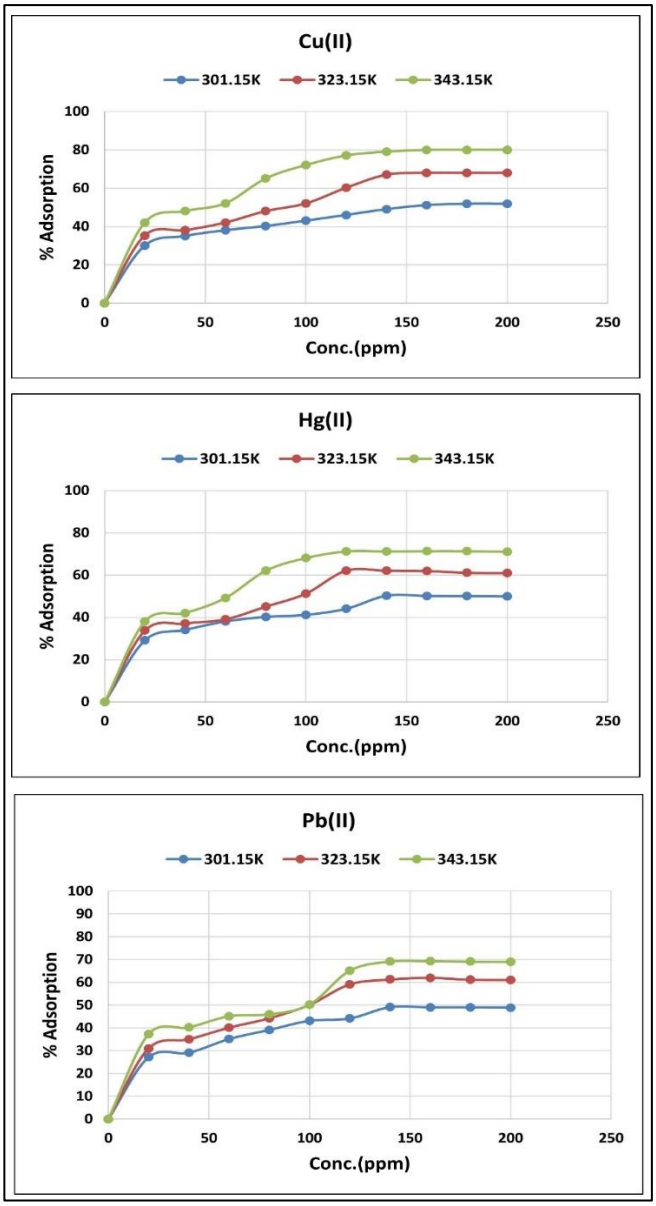

Fig 7 Isotherm of Adsorption of Metal Ions with Varying Initial Metal Ion Concentration

ISSN No:-2456-2165 https://doi.org/10.38124/ijisrt/26may1642

- *Variation of Adsorbent Dose*

Figure 8 represents the dependence of percentage adsorption of metal ions on the amount of Br-SOD used. As the amount of Br-SOD increased, the percentage removal of metal ions also increased. However, further increase in the amount of Cl-SoD did not produce any considerable increase in the percentage removal of metal ions. This behaviour can be explained by the number of metal ions available at a fixed initial concentration in the aqueous medium and the number of vacant adsorption sites on Br-SOD. As the amount of Br-SOD increases, the number of vacant sites on its surface also increases, thereby enhancing adsorption. However, beyond a certain adsorbent dose, although the number of vacant sites continues to increase, the number of metal ions remaining in the solution becomes comparatively less than the available adsorption sites. Under such conditions, a sufficient driving force for further adsorption is not developed. Consequently, the adsorption reaches a maximum value and thereafter remains nearly constant.

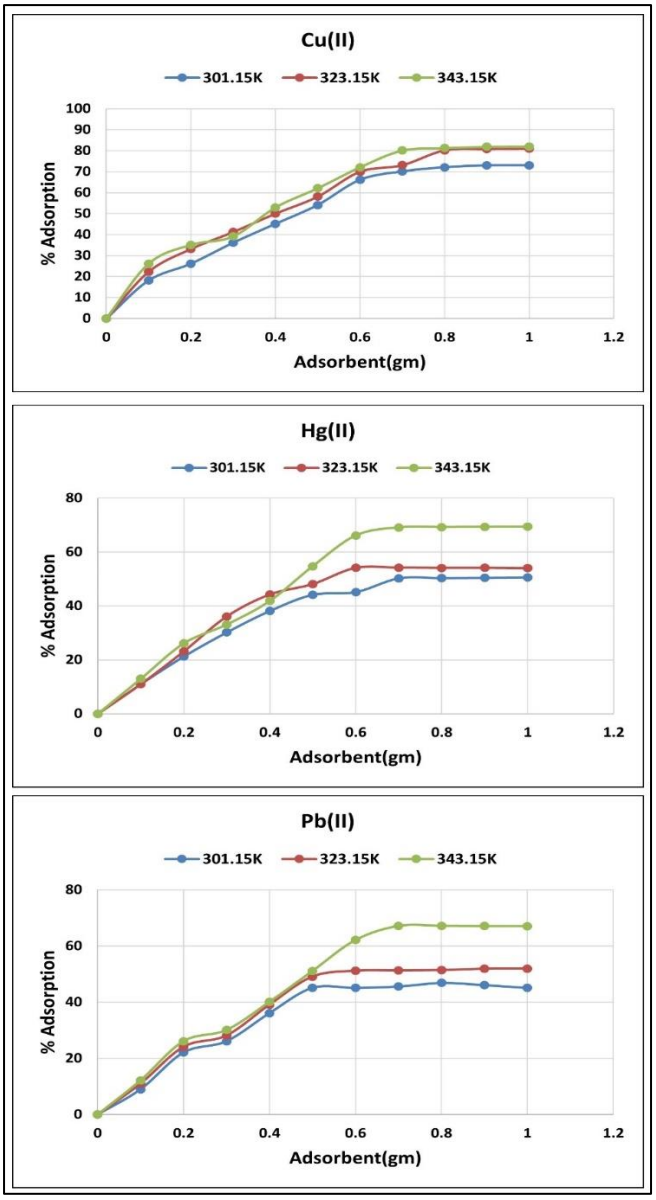

Fig 8 Isotherm of Adsorption of Metal Ions with Varying Adsorbent Dose

IV. CONCLUSION

This study shows that Br-SOD derived from coal fly ash is an effective and challenging material for removing metal ions from water. It was successfully synthesised from coal fly ash, providing a cost-effective and eco-friendly means of reusing industrial waste. Characterization confirmed the formation of bromosodalite with appropriate structure and surface features that enable efficient adsorption. Experimental results further demonstrated its outstanding ability to adsorb specific metal ions. Br-SOD showed the highest affinity towards Cu^{2+} ions among the three metal ions, demonstrating greater selectivity and a stronger interaction with copper compared to the others. Its greater adsorption capacity likely stems from its mesoporous structure, active sites, and ion exchange properties. Additionally, the adsorption experiments indicated that factors such as adsorbent dose, pH, and temperature play significant roles in the process. An increase in temperature led to a higher percentage of adsorption, suggesting that the adsorption process is endothermic. Higher temperatures possibly enhance the kinetic energy of metal ions and increase the accessibility of active adsorption sites, thereby improving adsorption efficiency. The results clearly indicate that coal fly ash derived Br-SOD possesses excellent adsorption characteristics and can be effectively used as a low-cost and eco-friendly adsorbent for the removal of heavy metal ions, particularly Cu^{2+} ions, from wastewater.

REFERENCES

[1]. Swain CK. Environmental pollution indices: a review on concentration of heavy metals in air, water, and soil near industrialization and urbanisation. *Discover Environment*. 2024;2:5. doi:10.1007/s44274-024-00030-8.

[2]. Khan M, et al. Comprehensive review on toxic heavy metals in the aquatic system: sources, identification, treatment strategies, and health risk assessment. *Environmental Research*. 2024;258:119440. doi:10.1016/j.envres.2024.119440.

[3]. Singh V, et al. Toxic heavy metal ions contamination in water and their sustainable reduction by eco-friendly methods: isotherms, thermodynamics and kinetics study. *Scientific Reports*. 2024;14:7595. doi:10.1038/s41598-024-58061-3.

[4]. Joshi AA, Chaudhari K, Ragupathy G. Recent trends in heavy metal removal technologies from water: mechanisms and advancements. *Environmental Science: Water Research & Technology*. 2026;12:421-456. doi:10.1039/D4EW01024H.

[5]. Murtaza G, et al. Heavy metal pollution in the aquatic environment: efficient and low-cost removal approaches to eliminate their toxicity: a review. *RSC Advances*. 2023;13:17540-17570. doi:10.1039/D3RA00723E.

[6]. Jorge AOS, et al. Recent developments in the removal of heavy metals from water and wastewater. *Proceedings*. 2024;105(1):122. doi:10.3390/proceedings2024105122.

[7]. Patil S, et al. Advanced strategies to mitigate heavy metals in ground and sewage water. *Current Opinion in Green and Sustainable Chemistry*. 2024;47:100917. doi:10.1016/j.cogsc.2024.100917.
[8]. Patel P, et al. A systematic review on heavy metal contamination in sediment, water, and different faunal groups inhabiting marine waters of India. *Water Environment Research*. 2025. doi:10.1002/wer.70194.
[9]. Alabssawy AN, Hashem AH. Bioremediation of hazardous heavy metals by marine microorganisms: a recent review. *Archives of Microbiology*. 2024;206:103. doi:10.1007/s00203-023-03793-5.
[10]. Pillay K, et al. A comprehensive review of heavy metals (Pb2+, Cd2+, Ni2+) removal from wastewater using low-cost adsorbents. *Environmental Technology*. 2024. doi:10.1080/09593330.2024.2358450.
[11]. Xu X, Pan J, Zhang H, Lin H. Progress in remote sensing of heavy metals in water. *Remote Sensing*. 2024;16(20):3888. doi:10.3390/rs16203888.
[12]. Adeleye AT, et al. The unseen threat of the synergistic effects of microplastics and heavy metals in aquatic environments: a critical review. *Current Pollution Reports*. 2024;10:478-497. doi:10.1007/s40726-024-00298-7.
[13]. Machado AA, Valiaparampil JG, Lavanya M. Unlocking the potential of algae for heavy metal remediation. *Water Air Soil Pollut*. 2024;235:629. doi:10.1007/s11270-024-07436-3.
[14]. Flores-Ramírez R, et al. Association between lead source exposure and blood lead levels in some lead manufacturing countries: a systematic review and meta-analysis. *J Trace Elem Med Biol*. 2022;71:126948. doi:10.1016/j.jtemb.2022.126948.
[15]. Kinally C, et al. A review of lead exposure source attributional studies. *Sci Total Environ*. 2025;990:179838. doi:10.1016/j.scitotenv.2025.179838.
[16]. Wani AL, Ara A, Usmani JA. Lead toxicity: a review. *Interdiscip Toxicol*. 2015;8(2):55-64. doi:10.1515/intox-2015-0009.
[17]. Tchounwou PB, et al. Heavy metals toxicity and the environment. *EXS*. 2014;101:133-164. doi:10.1007/978-3-7643-8340-4_6.
[18]. National Academies of Sciences, Engineering, and Medicine. *Investigative strategies for lead-source attribution at Superfund sites associated with mining activities*. Washington (DC): National Academies Press; 2017. doi:10.17226/24898.
[19]. O'Connor D, et al. Lead-based paint remains a major public health concern: a critical review of global production, trade, use, exposure, health risk, and implications. *Environ Int*. 2018;121:85-101. doi:10.1016/j.envint.2018.08.052.
[20]. Sampson MM, et al. Single-cell investigation of lead toxicity from neurodevelopment to neurodegeneration: current review and future opportunities. *Curr Opin Toxicol*. 2024;38:100464. doi:10.1016/j.cotox.2024.100464.
[21]. Upadhyay K, et al. Association between chronic lead exposure and markers of kidney injury: a systematic review and meta-analysis. *Toxicol Rep*. 2024;13:101837. doi:10.1016/j.toxrep.2024.101837.
[22]. Parithathvi A, Choudhari N, Dsouza HS. Prenatal and early life lead exposure induced neurotoxicity. *Hum Exp Toxicol*. 2024. doi:10.1177/09603271241285523.
[23]. Veeraswamy D, et al. Exploring the origins and cleanup of mercury contamination: a comprehensive review. *Environ Sci Pollut Res*. 2024;31(41):53943-53972. doi:10.1007/s11356-023-30636-z.
[24]. Rahman MM, et al. Mercury in groundwater – source, transport and remediation. *Appl Geochem*. 2024;170:106060. doi:10.1016/j.apgeochem.2024.106060.
[25]. Aldous AR, Tear T, Fernandez LE. The global challenge of reducing mercury contamination from artisanal and small-scale gold mining (ASGM): evaluating solutions using generic theories of change. *Ecotoxicology*. 2024;33:506-517. doi:10.1007/s10646-024-02785-5.
[26]. Liu Q, et al. Bibliometric analysis on mercury emissions from coal-fired power plants: a systematic review and future prospect. *Environ Sci Pollut Res*. 2024;31:19148-19165. doi:10.1007/s11356-024-32369-z.
[27]. Kang B, Wang J, Guo S, Yang L. Mercury-induced toxicity: mechanisms, molecular pathways, and gene regulation. *Sci Total Environ*. 2024;943:173577. doi:10.1016/j.scitotenv.2024.173577.
[28]. Jeong H, et al. Toxicity of methylmercury in aquatic organisms and interaction with environmental factors and coexisting pollutants: a review. *Sci Total Environ*. 2024;943:173574. doi:10.1016/j.scitotenv.2024.173574.
[29]. Fioravanti R, et al. Bioaccumulation and biomagnification of mercury along the seafood chain in Europe: a systematic review. *Foods*. 2025;14(21):3752. doi:10.3390/foods14213752.
[30]. Shen X, et al. Simultaneous Cu(II)-EDTA decomplexation and Cu(II) recovery using integrated contact-electro-catalysis and capacitive deionization from electroplating wastewater. *J Hazard Mater*. 2024;472:134548. doi:10.1016/j.jhazmat.2024.134548.
[31]. Hao C, Wang A. Adsorption of Cu2+, Ni2+, and Cr(VI) heavy metal ions on sodium hexatitanate nanorods from industrial electroplating wastewater assisted by calcium hypochlorite oxidation. *Ind Eng Chem Res*. 2024;63(40):16990-17005. doi:10.1021/acs.iecr.4c02711.
[32]. Ma J, Xiong Z. Sustainable metal recovery from electroplating sludge: bridging technology and environmental regulation. *Sustainability*. 2025;17(11):4957. doi:10.3390/su17114957.
[33]. Mebarki A, et al. Comparing conventional and advanced approaches for heavy metal removal in wastewater treatment: an in-depth review emphasizing filter-based strategies. *Polymers*. 2024;16(14):1959. doi:10.3390/polym16141959.
[34]. Brião GV, et al. Electrochemical processes for the treatment of contaminant-rich wastewater: a comprehensive review. *Chemosphere*.

2024;355:141884. doi:10.1016/j.chemosphere.2024.141884.
[35]. Twizerimana P, Wu Y. Overview of integrated electrocoagulation-adsorption strategies for the removal of heavy metal pollutants from wastewater. *Discover Chemical Engineering*. 2024;4:14. doi:10.1007/s43938-024-00053-w.
[36]. Khanzada AK, et al. Hydrochar as a bio-based adsorbent for heavy metals removal: a review of production processes, adsorption mechanisms, kinetic models, regeneration and reusability. *Sci Total Environ*. 2024;945:173972. doi:10.1016/j.scitotenv.2024.173972.
[37]. Essalmi S, et al. Design and application of metal organic frameworks for heavy metals adsorption in water: a review. *RSC Adv*. 2024;14:9365-9390. doi:10.1039/D3RA08815D.
[38]. Nworie FS, et al. Heavy metals removals from wastewater and reuse of the metal loaded adsorbents in various applications: a review. *Hybrid Advances*. 2024;6:100193. doi:10.1016/j.hybadv.2024.100193.
[39]. Xie S. Biosorption of heavy metal ions from contaminated wastewater: an eco-friendly approach. *Environ Technol Rev*. 2024. doi:10.1080/17518253.2024.2357213.
[40]. Chukanov NV, Aksenov SM. Structural features, chemical diversity, and physical properties of microporous sodalite-type materials: a review. *Int J Mol Sci*. 2024;25(18):10218. doi:10.3390/ijms251810218.
[41]. Linhong J, et al. Research progress on adsorption of heavy metal ions in wastewater by zeolitic imidazolate framework-based nanomaterials. *New Chem Mater*. 2024;52(12):245-250. doi:10.19817/j.cnki.issn1006-3536.2024.12.012.
[42]. Azeez A, et al. ZIF-67-based materials as adsorbent for liquid phase adsorption: a review. *Polyhedron*. 2024;260:117069. doi:10.1016/j.poly.2024.117069.
[43]. Yadav V, et al. Coal fly ash utilization in environmental remediation and sustainable materials development: a review. *J Environ Manage*. 2024;368:122203. doi:10.1016/j.jenvman.2024.122203.
[44]. Wang S, Peng Y. Natural zeolites as effective adsorbents in water and wastewater treatment. *Chem Eng J*. 2024;495:153420. doi:10.1016/j.cej.2024.153420.
[45]. Alhokbany N, et al. Synthesis of zeolite materials from coal fly ash for wastewater treatment applications: recent advances and challenges. *Mater Today Sustain*. 2024;26:100742. doi:10.1016/j.mtsust.2024.100742.
[46]. Musyoka NM, et al. Sustainable synthesis of zeolites from coal fly ash and their environmental applications. *Appl Clay Sci*. 2024;258:107451. doi:10.1016/j.clay.2024.107451.
[47]. Ghorpade SB, Patil RP, Borhade AV. Hydrothermal synthesis of a solid acid catalyst based on bromosodalite and its application in esterification. *J Adv Chem Sci*. 2026;12(4):995-998. doi:10.30799/jacs.S305.26120405.